Strathprints Institutional Repository

Structural and magnetic study of Yb^{3+}

in the perovskites Sr_2YbMO_6 (M = Nb, Ta, Sb)

Fiona C. Coomer,[1] John Campbell, Nico Giordano, Oonagh M. Collins, Edmund J. Cussen*

WestCHEM, Department of Pure and Applied Chemistry,

University of Strathclyde,

295 Cathedral Street,

Glasgow, G1 1XL

United Kingdom

E-mail: edmund.cussen@strath.ac.uk

Tel: +44 141 548 2797

[1] *Present Address:*

ISIS Neutron and Muon Source, STFC Rutherford Appleton Laboratory,
Harwell Science and Innovation Campus, Didcot, Oxfordshire OX11 0QX, UK

Abstract

The compounds Sr_2YbNbO_6, Sr_2YbTaO_6 and Sr_2YbSbO_6 have been prepared using solid state methods by heating pelleted reagents in air at temperatures up to 1400°C. Rietveld refinement against room temperature neutron powder diffraction data show that all three compounds crystallise with a cation-ordered variant of the perovskite structure in the $P2_1/n$ space group. Complete cation ordering occurs between M^{5+} and Yb^{3+} over two octahedrally-coordinated sites in the structure and all compounds are stoichiometric in oxygen. The Sb-O bond lengths are similar to related perovskite compounds but differ slightly from those indicated by bond valence sums. Magnetic susceptibility data resemble Curie-Weiss paramagnetic behaviour, but can be better understood as arising from the effect of the octahedral crystal field on the $^2F_{5/2}$ ground state of Yb^{3+} leading to a temperature dependent magnetic moment on this ion below 100 K.

Introduction

The perovskite structure undergoes a large number of distortions that allow the accommodation of considerable variation in cation sizes and charges.[1] In addition, when two cations of sufficient difference in size and/or charge occupy the octahedrally-coordinated sites in the structure then cation ordering may also occur. The most common form of ordering leads to an alternating arrangement of cations on these sites and so results in a rock-salt type face-centred cubic (*fcc*) substructure. There is considerable interest in such cation ordering as the *fcc* lattice contains nearest neighbouring cations arranged on regular edge-sharing tetrahedra.[2-5] Consequently antiferromagnetic interactions between moments on these lattice points cannot be satisfied by any collinear ordering in a long-range ordered antiferromagnetic structure. Instead a number of exotic magnetic states exist at low temperatures.[6-10] Interest has mainly focussed on magnetic ions where the unpaired electrons reside in the *d*-orbitals in order to give relatively strong superexchange interactions between the sites of the *fcc* lattice.

A number of cation-ordered perovskites have used lanthanide Ln^{3+} ordering with Mo^{5+} to access a range of physical behaviour. For the larger lanthanides the structure is tetragonally distorted at higher temperatures due to Ba^{2+} being too small to match the Goldschmidt radius for a cubic perovskite.[11] Both Ba_2NdMoO_6 and Ba_2SmMoO_6 exhibit a distortion of the MoO_6 octahedra with two short Mo-O and four longer Mo-O bonds that partially stabilise the $4d^1$ electronic configuration.[11-12] Ba_2GdMoO_6 undergoes a transition from cubic to tetragonal symmetry at 220 K before undergoing a ferroelastic distortion to a triclinically-distorted phase at 80K.[13] For the smaller lanthanides the compounds exhibit the undistorted face-centred cubic structure.[11] Where Ln^{3+} is a diamagnetic cation such as Y^{3+} or Lu^{3+} this gives a face-centred array of $4d^1$ Mo^{5+} cations with no other paramagnetic species present in the compound.[10-11] Antiferromagnetic coupling between nearest neighbours on such a lattice leads to geometric frustration due to the formation of regular tetrahedra of mutual interactions that cannot be simultaneously satisfied.

The antiferromagnetic coupling in the series Ba_2LnMoO_6 shows a large variation in magnitude from *ca.* -130 to -8 K. Ba_2YMoO_6[8-9, 11] and Ba_2LuMoO_6 [10] show strong coupling with Weiss constants of *ca.* -130 K but the formation of a long range antiferromagnetically ordered state is supressed due to the frustrated *fcc* lattice.[11] Instead, a loss of the bulk magnetic moment is observed on cooling along with a reduction in the electronic entropy and a Knight shift in the [89]Y NMR suggesting[8-9] that this arises from the formation of a valence bond state. This assignment has been confirmed by the observation of an excitation from the $S=^1/_2$ spin singlet ground state in Ba_2YMoO_6.[14] The

paramagnetic species Er^{3+} has a similar size to the diamagnetic cations Y^{3+} and Lu^{3+}, and Ba_2ErMoO_6 has the same cubic structure, but shows only weak antiferromagnetic coupling with a Weiss constant $\approx$ -10 K.[15] This can be contrasted with the isostructural compound Ba_2YbMoO_6 which has a Weiss constant that is an order of magnitude larger, -116 K.[11]

The variation in physical behaviour from valence bond glass, to ferroelastic phase transitions, to Jahn-Teller distortions provide strong evidence that subtle variations in the chemistry of the Ln^{3+} bonding have an important impact on the physical properties of the series Ba_2LnMoO_6. The effect of the crystal field on lanthanide cations can be significant at very low temperature, as shown in Ba_2HoSbO_6, but even in this case the magnetic behaviour at high temperature suggests Curie-Weiss paramagnetism with weak ($\theta= -7.7$ K) antiferromagnetic coupling between Ho^{3+} cations.[6]

We have examined the role of the $4f$ orbitals in these systems by preparing diamagnetic analogues of the Mo^{5+} compounds. Here we report three compounds where the only paramagnetic species is the Yb^{3+} cation and so examine the magnetic interactions between Yb^{3+} cations occupying the points of the distorted fcc lattice shown in Figure 1. Neutron diffraction has been used to accurately determine the structure of three new compounds, and a Curie-Weiss analysis of the magnetic susceptibility would suggest surprisingly strong interactions between the $4f^{13}$ centres. Here we show that the magnetic susceptibility can better be explained by the subtle effect of the crystal field on the isolated $4f$ orbitals.

Experimental

Polycrystalline samples were prepared from stoichiometric mixtures of reagents using conventional solid state methods. All reagents had a purity of not less than 99.99 %. Strontium carbonate, ytterbium oxide and niobium- tantalum- or antimony-(V) oxide were ground in a mortar and pestle and then pressed into pellets of 13 mm diameter under a load of *ca*. 2 tonnes. The pellets were then heated at 800^oC for 1 day. The samples were then ground, repelleted and heated in air at a number of temperatures increasing up to 1400^oC. Due to the slow rate of product formation the samples were reground up to ten times and the total heating times amounted to around 30 days. Alternative sol gel preparations[16] gave an initially more rapid product formation but did not achieve a pure sample any more rapidly than the conventional ceramic route.

X-ray powder diffraction was used to follow the progress of the reaction. Data were collected in Bragg Brentano geometry using a Panalytical Xpert diffractometer operating with Cu Kα radiation.

Neutron diffraction data were collected using the time-of-flight high-resolution powder diffractometer (HRPD) at the ISIS spallation source at the Rutherford Appleton Laboratories, Didcot, U.K. For these experiments *ca*. 5 g of sample was contained in a cylindrical vanadium can, with an internal diameter of 11 mm. Diffraction patterns were recorded over the time-of-flight range 30–130 ms in back-scattering and 90° detector banks, in order to sample a d-spacing range from 0.6 to 3.9 Å. Data analysis used the Rietveld method[17] of structure refinement as implemented in the GSAS suite of programs.[18-19] Refinements were carried out simultaneously against both banks of data. An empirical fit to the background was carried out using shifted Chebyshev functions and a convolution of exponential and pseudo Voigt functions was used to model the profile of the Bragg peaks.

Magnetic data were collected using a Quantum Design SQUID magnetometer. Around 100 mg of each sample was accurately weighed into gelatin capsules and data were recorded after cooling the samples in either the measuring field of 100, 1000 or 5000 G or zero applied field. Data were corrected for diamagnetism of the sample, but this had no significant effect on the size of the susceptibility. Bond valence sums were determined using the parameters derived from a library of metal oxides.[20]

Results

X-ray powder diffraction data collected from each of the three compositions contained the peaks associated with the primitive perovskite structure with lattice parameter $a_p \approx 4.1$ Å, but showed additional reflections and peak splitting indicative of cation-ordering between the M^{5+} and Yb^{3+} cations and a reduction in metric symmetry from the classic cubic perovskite model. Due to the dominance of the X-ray scattering by the cations, neutron diffraction was necessary to give an accurate description of the oxide anion displacements that are commonly the main manifestation of the reduction in symmetry in perovskite structures.[6, 21] The high resolution neutron diffraction data from each composition showed unambiguous peak splitting associated with a metrically monoclinic unit cell related to the primitive cubic perovskite cell by the expansion $a' \approx a_p\sqrt{2}$, $b' \approx a_p\sqrt{2}$, $c' \approx 2a_p$ and $\beta \approx 90°$. The neutron diffraction data were fitted using the monoclinically distorted cell with $P2_1/n$ symmetry. The lattice parameters remain close to those from metrically higher symmetry cells, such as the $GdFeO_3$ structure,[22] but the lower symmetry can be clearly identified by examining the tilting of the oxide octahedra. For each compound the diffracted intensity can only be reproduced by allowing tilting of the octahedra about three axes in the $a^-a^-c^+$ mode outlined in the Glazer scheme.[23] The octahedral tilting in these structures and the marginal displacement of the Yb^{3+} sublattice are illustrated in Figure 1.

Refinement of the atomic positions readily produced a reasonable fit to the data. This structural model contains two octahedrally-coordinated sites of distinctly different sizes. Trial refinements indicated that the larger site is exclusively occupied by Yb^{3+}. Unconstrained refinement of the site occupancy of all of the oxide positions did not provide any improvement to the quality of the fit and refined to values within a standard deviation of unity for each of the three oxide positions. As these diffraction data indicate full occupancy and order, the final refinements were carried out with complete cation ordering and full oxide site occupancy. Trial refinement of the displacement parameters of the Yb^{3+} and M^{5+} cations yielded slightly negative isotropic factors that were within one standard deviation of zero for Sr_2YbTaO_6 and Sr_2YbSbO_6. Fixing these at the positive values observed for Sr_2YbNbO_6 resulted in no significant deterioration of the quality of fit and so the thermal displacement of these cations was fixed at these physically meaningful (i.e. positive) values. Two extremely weak, unindexed peaks at 2.1 and 3.0 Å were observed in each of the data sets. These could not be matched to possible impurities and, due to the absence of overlap with Bragg peaks from the monoclinic perovskite and the absence of additional peaks at shorter d-spacings these do not perturb the structural refinement. As can be seen in

Figure 2, the data from each sample could be satisfactorily fitted. The resultant structural parameters are presented in Table 1 and the bond lengths in the metal-oxide octahedra are given in Table 2. The lattice parameters and bond angles indicative of the size of the distortion are collected in Figures 3 and 4 respectively. The structure of Sr_2YbNbO_6 is in agreement with a previous report[14] of composition $SrYb_{0.5}Nb_{0.5}O_3$ and our data provide enhanced precision in the estimates of the oxide positions.

Magnetic measurements down to 2 K in a range of magnetic fields from 100 G to 5000 G show a magnetic susceptibility that is independent of magnetic field over the full temperature range and show an increase on cooling that is characteristic of localised paramagnetic behaviour. None of the data provided any indication of a magnetic transition and the susceptibilities evolve smoothly as shown in Figure 5. The data were fitted to the Curie-Weiss law in the temperature range $300 \geq T/K \geq 150$ as shown in Figure 5 suggesting strong antiferromagnetic coupling with a Weiss constant of around -120 K. Similar observations have been made in $Cs_2NaYbCl_6$ and a Weiss constant of -70 K gave a good fit to those data.[24] However, the behaviour of $Cs_2NaYbCl_6$ is better rationalised by instead considering the effects of the octahedral crystal field on the $^2F_{7/2}$ ground state of Yb^{3+} ions that are wholly isolated from one another.

The ligand field splits the $^2F_{7/2}$ state into a Γ_6 ground state with either a Γ_8 or Γ_7 state slightly higher in energy. At high temperatures this splitting can be neglected, but at low temperature the population of these states is temperature dependent and is described by equation (1):[24]

$$\chi = \frac{N\beta^2}{3kT} \frac{g^2 S(S+1) + rf^2 \exp\left(-\frac{\Delta}{kT}\right)}{1 + r\exp\left(-\frac{\Delta}{kT}\right)} + b \qquad \text{Equation (1)}$$

where g is the gyromagnetic ratio for the Γ_6 ground state, r is the ratio of multiplicities of the excited state to the ground level , f^2 is the product of the gyromagnetic ratio and the spin for the excited level, S is the spin of the unpaired electron of the $4f^{13}$ ion, β is the Bohr magneton, Δ is the energy gap between the ground and excited states, N is Avogadro's number and k is the Boltzmann constant. A temperature independent paramagnetic (TIP) contribution is modelled by b.

Using the literature values[24] for the possible Γ_8 and Γ_7 states we fixed all parameters at those determined for Yb^{3+} in $Cs_2NaYbCl_6$ and allowed the TIP term to vary in order to reproduce the magnetic susceptibilities observed for Sr_2YbMO_6. This reproduced the susceptibility in the range 2-100 K as shown in Figure 6 with a marginally better fit being afforded by the Γ_7 excited state rather than the alternative Γ_8. The only variable used to fit the data was the temperature independent term that

refined to a value of $0.0074(2)$ cm^3 mol^{-1} that differs slightly from the value $0.0060(2)$ cm^3 mol^{-1} observed in $Cs_2NaYbCl_6$.

Discussion

High resolution neutron diffraction data show that the three compounds Sr_2YbMO_6 are isostructural and adopt a monoclinically-distorted variant of the perovskite structure. This is a consequence of cation ordering between Yb^{3+} and M^{5+}, and the Sr^{2+} cation being too small to occupy the interstice in the centre of a cubic structure. The bonding requirements of Sr^{+2} can be empirically evaluated using bond valence sums[20] that indicate reasonable agreement with the valence expected for divalent cation in a slightly underbonded, distorted environment with valences of 1.87, 1.87 and 1.84 for Sr_2YbNbO_6, Sr_2YbTaO_6 and Sr_2YbSbO_6 respectively. The structural data clearly indicate that cation ordering occurs between the M^{5+} and Yb^{3+} cations across octahedrally-coordinated sites of differing sizes as illustrated in Figure 1. The monoclinic structural distortion is most readily visualised as a tilting of the MO_6 octahedra about three different axes in the structure, $a^-a^-c^+$ in Glazer notation.[23] These octahedra are tilted at angles in the range 25 to 21° with the distortion in Sr_2YbSbO_6 being slightly less than Sr_2YbNbO_6 and Sr_2YbTaO_6 as shown in Figure 4. The tilting in each of these three phases is close to that reported previously in Sr_2ErMoO and Sr_2YMoO_6[15, 25] which both show tilts in the range 25 to 22°.

The distortion of the cubic structure to monoclinic symmetry leads to three pairs of crystallographically inequivalent oxide ions around each of the Yb/*M* cations. However, the bond lengths and angles remain close to those of regular octahedra. The Yb-O bond lengths of *ca*. 2.19 Å are similar to those encountered in related double perovskites,[11] but slightly shorter than expected given the Yb^{3+} radius of 0.868 Å.[26]

The bond lengths within the TaO_6 and NbO_6 octahedra are as expected for Ta^{5+} and Nb^{5+}. However, the Sb-O distances are somewhat long for a cation with a radius of 0.60 Å compared to those of Ta^{5+} and Nb^{5+} which both have radii of 0.64 Å.[26] Anomalous behaviour by Sb^{5+} is also clearly shown by comparing the bond valence sums of 4.93 and 5.01 for Nb and Ta with a value of 5.34 for Sb^{5+} that indicates that the Sb-O environment is more compressed than predicted. A small survey of related double perovskite phases Sr_2MSbO_6 and Ba_2MSbO_6 shows that bond valence sums of >5.2 are obtained for a range of compounds with *M* = Sc, In, Y, Ho.[27-30] These values come from cubic perovskites as well as rhombohedrally- and monoclinically-distorted variants and indicate that the effective radius of Sb^{5+} in these phases may be slightly smaller than the bond valence parameters suggest.

Magnetic susceptibility measurements show that data collected after cooling the sample in an applied field show no divergence from data collected after cooling in zero applied field. This absence of any

history dependence suggests that the magnetic moments remain dynamically disordered down to 2 K and so are able to partially align with the applied magnetic field. For temperatures $\geq$150 K the data were initially fitted using the Curie-Weiss law that describes the interaction between localised magnetic moments. The moments derived from these fits of *ca.* 4.8 μ_B is slightly larger than the value of 4.54 μ_B anticipated from the full spin and orbit contribution arising from the $^2F_{7/2}$ ground state of Yb^{3+}. However, this fit requires an unfeasibly strong coupling between the Yb centres as indicated by a Weiss constant of $\theta \approx$ -120 K.

The shortest Yb^{3+}... Yb^{3+} distance in Sr_2YbMO_6 is a through-space distance of $\approx$ 5.8 Å although the superexchange pathway involves the Yb–O–*M*–O–Yb interaction and requires orbital overlap to occur over a distance of *ca.* 8.2 Å. Due to this extended distance and the withdrawn nature of the 4*f* orbitals it would be anticipated that the magnetic coupling between Yb^{3+} centres would be extremely weak.

This exceptional behaviour of Yb^{3+} compared to other Ln^{3+} cations has also been observed in the series of compounds $SrLn_2O_4$ where for Gd^{3+}, Dy^{3+}, Ho^{3+} and Er^{3+} the weak antiferromagnetic interactions between Ln^{3+} cations led to Weiss constants in the range -9 to -13 K.[31] However, the apparent antiferromagnetic coupling in $SrYb_2O_4$ is an order of magnitude stronger with a value of θ = -99 K. An alternative explanation for the temperature dependence is sought and the data from Sr_2YbMO_6 can instead be rationalised as arising from isolated Yb^{3+} centres in the lattice.

The single ion behaviour of Yb^{3+} is well understood and the lowest lying excited state ($^2F_{5/2}$) is around 10 000 cm^{-1} higher[32] in energy that the $^2F_{7/2}$ ground state. This is equivalent to kT for *ca.* 14×10^3 K and so is not thermally accessible. However, the modest effect of the octahedral arrangement of oxide ions is sufficient to modify the magnetic properties of the Yb^{3+} cation at low temperatures by splitting the $^2F_{7/2}$ state. This gives a lowest magnetic state Γ_6 with Γ_7 and Γ_8 excited states 45 and 60 cm^{-1} higher in energy respectively.[24] The apparent Curie-Weiss behaviour observed above 150 K is due to the Yb^{3+} moment being dependent on the population of these levels. This assignment is supported by the data below 100 K that show that the magnetic moment is partitioned as expected between the split states. The data show a slightly better agreement with the prediction of the Γ_7 as the lowest lying excited state.

This interpretation of Yb^{3+} cations that behave as predominantly isolated ions is in keeping with observations from related compounds such as the cubic perovskite Ba_2HoSbO_6.[5] Ba_2HoSbO_6 shows important crystal field effects on the magnetic properties below 10 K, and at higher temperatures shows only weak antiferromagnetic coupling in the Curie-Weiss regime (θ = -7.7K).

Conclusions

Cation ordering between Yb^{3+} and M^{5+} results in Sr_2YbNbO_6, Sr_2YbTaO_6 and Sr_2YbSbO_6 crystallising with the cation-ordered distorted perovskite structure with tilting of the oxide octahedra about three axes. Despite the distortion from ideal cubic symmetry, the similarity in tilt angles of the oxide octahedra means that the frustrated geometry of the face-centred Yb^{3+} sub-lattice is largely preserved. This arrangement of octahedrally-coordinated cations presents a model system to investigate the interactions between Yb^{3+} cations in frustrated antiferromagnetic oxides. A Curie-Weiss analysis of the magnetic behaviour would suggest that the coupling between Yb^{3+} centres is considerably stronger than shown in related perovskites containing similarly-sized Ln^{3+} cations such as Ho^{3+} and Er^{3+} [6, 15] Instead, the data are indicative of a temperature dependent effective magnetic moment and the magnetic susceptibility can be reproduced by modelling the effect of the octahedral crystal field on the $^2F_7$ ground state of the magnetically-isolated Yb^{3+} cations.

Supplementary Information: Full crystallographic details, interatomic parameters and bond valence calculations are listed in electronic supplementary information.

Figure 1 a) The cation-ordered perovskite structure exhibited by Sr_2YbMO_6. Grey spheres show Sr^{2+} cations whilst yellow and red octahedra represent YbO_6 and $Nb/Ta/SbO_6$ units respectively. The distortion from cubic symmetry lifts the degeneracy of the pseudo face-centred cubic (*fcc*) lattice of Yb^{3+} centres, although as indicated by the distances shown in (b) the tilting of the octahedra leads to minimal distortion in the tetrahedra that compose the pseudo-*fcc* lattice. The pseudo-*fcc* lattice is composed of Yb^{3+} centres as indicated by black spheres in (b).

Figure 2 Neutron time-of-flight powder diffraction patterns collected at room temperature from: (a) and (b) Sr_2YbNbO_6, (c) and (d) Sr_2YbTaO_6, (e) and (f) Sr_2YbSbO_6. Observed and calculated diffraction profiles are represented by dots and a solid line respectively. The structures were refined against two data banks simultaneously and the difference curve is illustrated.

Figure 3 The lattice parameters derived from neutron diffraction data collected at room temperature from Sr_2YbMO_6. The left axis indicates the values denoted by circles and squares for a and b respectively whilst c is represented by squares and the values shown on the right axis. The left and right axes are scaled such that $c/\sqrt{2}$ is comparable to the values a and b.

Figure 4 a) The $M-O-Yb$ angles that indicate the tilting of the oxide octahedra in Sr_2YbMO_6. Circles denote values from Sr_2YbTaO_6, squares correspond to Sr_2YbNbO_6 and values from Sr_2YbSbO_6 are shown as triangles.

Figure 5 Magnetic susceptibility data collected from: (a) and (b) Sr_2YbNbO_6, (c) and (d) from Sr_2YbTaO_6, (e) and (f) from Sr_2YbSbO_6. The inverse susceptibility is shown on the left to illustrate the agreement with the Curie-Weiss fit represented as a solid line. The Curie Weiss fit is entirely fortuitous and has no physical significance due to the temperature dependent magnetic moment of Yb^{3+}. Data were collected after cooling in zero applied field (circles) and after cooling in the measuring field of 1000 G (triangles).

Figure 6 The inverse magnetic susceptibility of Sr_2YbTaO_6 is compared with the susceptibility calculated for Yb^{3+} in an octahedral ligand field using literature values.[24, 33] The black line

represents the literature model based on splitting of the ground state $^2F_{7/2}$ into a Γ_6 ground state with a low lying Γ_7 level 45 cm^{-1} higher in energy. All parameters were fixed apart from the temperature independent term which refined from the value of 0.006(2) to 0.0075(2).

Table 1 Atomic coordinates for Sr_2YbMO_6 derived from refinement against neutron diffraction data collected at room temperature.

	atom	x	y	z	$100U_{iso}$
Sr_2YbNbO_6	Sr	0.0068(5)	0.0273(2)	0.2490(5)	1.07(3)
$P2_1/n$:	Nb	0	$^1/_2$	0	0.15(2)
a = 5.79020(7),	Yb	$^1/_2$	0	0	0.15(2)
b = 5.81748(6),	O(1)	0.2713(5)	0.2947(6)	0.0361(5)	1.02(9)
c = 8.20087(11) Å,	O(2)	0.3007(5)	0.2767(6)	0.4625(4)	0.84(8)
β = 90.110(1) °,	O(3)	0.9285(4)	0.4826(3)	0.2373(4)	0.86(5)
Vol. = 276.241(4) Å^3					
Sr_2YbTaO_6	Sr	0.0052(5)	0.0277(2)	0.2483(4)	0.57(2)
$P2_1/n$:	Ta	0	$^1/_2$	0	0.10*
a = 5.79147(6),	Yb	$^1/_2$	0	0	0.10*
b = 5.82054(5),	O(1)	0.2719(4)	0.2949(5)	0.0349(4)	0.95(7)
c = 8.20398(9) Å,	O(2)	0.3001(5)	0.2772(6)	0.4613(4)	0.71(7)
β = 90.113(1) °,	O(3)	0.9274(4)	0.4838(4)	0.2366(4)	0.31(4)
Vol. = 276.552(3) Å^3					
Sr_2YbSbO_6	Sr	0.0048(5)	0.0243(2)	0.2484(4)	0.41(2)
$P2_1/n$:	Sb	0	$^1/_2$	0	0.10*
a = 5.78749(7),	Yb	$^1/_2$	0	0	0.10*
b = 5.79994(7),	O(1)	0.2688(4)	0.2931(5)	0.0335(4)	0.85(8)
c = 8.18956(11) Å,	O(2)	0.2971(5)	0.2732(5)	0.4646(4)	0.50(7)
β = 90.136(1) °,	O(3)	0.9310(4)	0.4865(4)	0.2360(3)	0.09(4)
Vol. = 274.899(2) Å^3					

* Isotropic temperature factors were fixed at these values to avoid refinement to non−positive values that were within one standard deviation of zero.

Table 2 Selected interatomic distances in Å for Sr_2YbMO_6 derived from Rietveld refinement against neutron diffraction data collected at room temperature.

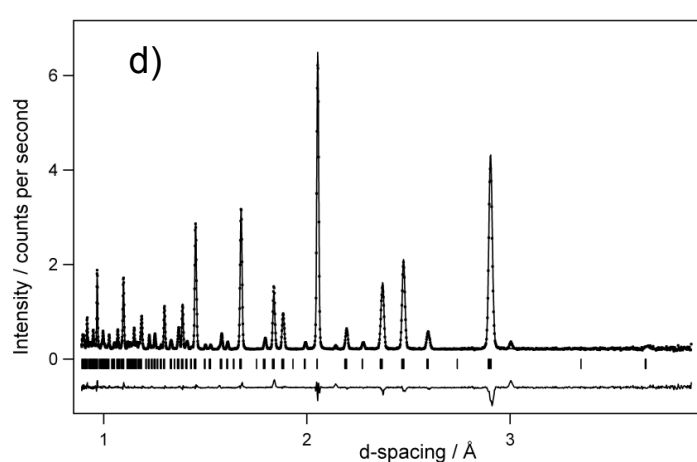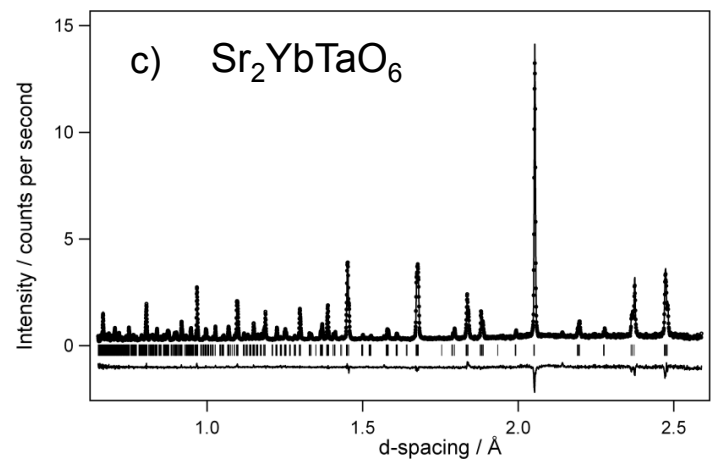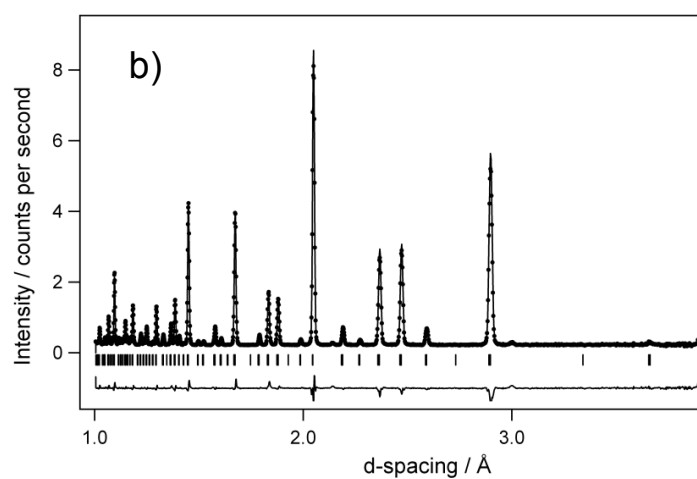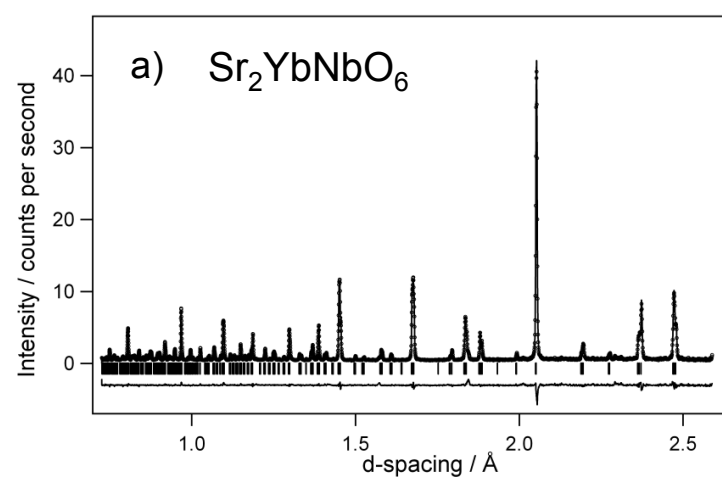| Sr_2YbNbO_6		Sr_2YbTaO_6		Sr_2YbSbO_6	
Nb-O(1)	1.995(3) × 2	Ta-O(1)	1.996(2) × 2	Sb-O(1)	1.983(2) × 2
Nb-O(2)	2.004(3) × 2	Ta-O(2)	2.011(3) × 2	Sb-O(2)	1.993(3) × 2
Nb-O(3)	1.993(4) × 2	Ta-O(3)	1.989(3) × 2	Sb-O(3)	1.976(3) × 2
Yb-O(1)	2.187(3) × 2	Yb-O(1)	2.185(3) × 2	Yb-O(1)	2.181(2) × 2
Yb-O(2)	2.194(3) × 2	Yb-O(2)	2.192(3) × 2	Yb-O(2)	2.185(3) × 2
Yb-O(3)	2.195(3) × 2	Yb-O(3)	2.202(3) × 2	Yb-O(3)	2.199(3) × 2

References

1. R. H. Mitchell, *Perovskites: Modern and Ancient*. Almaz Press: Thunder Bay, Ontario, 2002.

2. A. Harrison, *J. Phys.: Condens. Matter* **2004,** *16* (11), S553-S572.

3. J. E. Greedan, *J. Mater. Chem.* **2001,** *11*, 37-53.

4. J. E. Greedan, Geometrically Frustrated Magnetic Materials. In *Functional Oxides*, Bruce, D. W.; O'Hare, D.; Walton, R. I., Eds. John Wiley & Sons, Ltd.: Chichester, 2010; pp 41-109.

5. S. Calder; X. Ke; F. Bert; A. B. Amato, C.; C. Carboni; R. J. Cava; A. Daoud-Aladine; P. F. Deen, T.; A. D. Hillier; H. Karunadasa; J. W. Taylor; P. Mendels; P. Schiffer; S. T. Bramwell, *Phys. Rev. B* **2010,** *81*, 6.

6. F. C. Coomer; E. J. Cussen, *Inorg. Chem.* **2014,** *53*, 746-755.

7. S. T. Bramwell; M. J. P. Gingras; J. P. Michael, *Science* **2001,** *294* (5546), 1495-1501.

8. M. A. de Vries; A. C. McLaughlin; J. W. G. Bos, *Phys. Rev. Lett.* **2010,** *104* (17), 177202-4.

9. T. Aharen; J. E. Greedan; C. A. Bridges; A. A. Aczel; J. Rodriguez; G. MacDougall; G. M. Luke; T. Imai; V. K. Michaelis; S. Kroeker; H. D. Zhou; C. R. Wiebe; L. M. D. Cranswick, *Phys. Rev. B* **2010,** *81* (22), 224409.

10. F. C. Coomer; E. J. Cussen, *J. Phys.: Condens. Matter* **2013,** *25* (8), 082202.

11. E. J. Cussen; D. R. Lynham; J. Rogers, *Chem. Mater.* **2006,** *18*, 2855-2866.

12. A. C. Mclaughlin, *Phys. Rev. B* **2008,** *78*, 132404.

13. T. K. Wallace; R. H. Colman; A. C. McLaughlin, *PCCP* **2013,** *15*, 8672-8677.

14. C. Yang; L. Lee, *Acta Crystallogr., Sect. B: Struct. Sci* **1999,** *55* (3), 348-354.

15. E. J. Cussen, *J. Solid State Chem.* **2007,** *180* (2), 474-483.

16. P. D. Battle; T. C. Gibb; A. J. Herod; J. P. Hodges, *J. Mater. Chem.* **1995,** *5* (1), 75-78.

17. H. M. Rietveld, *J. Appl. Crystallogr.* **1969,** *2*, 65-71.

18. A. C. Larson; R. B. von Dreele *General Structure Analysis System (GSAS)*; Los Alamos National Laboratories: Los Alamos, NM, 1990.

19. B. H. Toby, *J. Appl. Crystallogr.* **2001,** *34*, 210-213.

20. N. E. Brese; M. O'Keeffe, *Acta Cryst.* **1991,** *B47*, 192-197.

21. P. W. Barnes; M. W. Lufaso; P. M. Woodward, *Acta Crystallogr., Sect. B: Struct. Sci* **2006,** *B62*, 384-396.

22. E. J. Cussen; M. J. Rosseinsky; P. D. Battle; J. C. Burley; L. E. Spring; J. F. Vente; S. J. Blundell; A. I. Coldea; J. Singleton, *J. Am. Chem. Soc.* **2001,** *123* (6), 1111-1122.

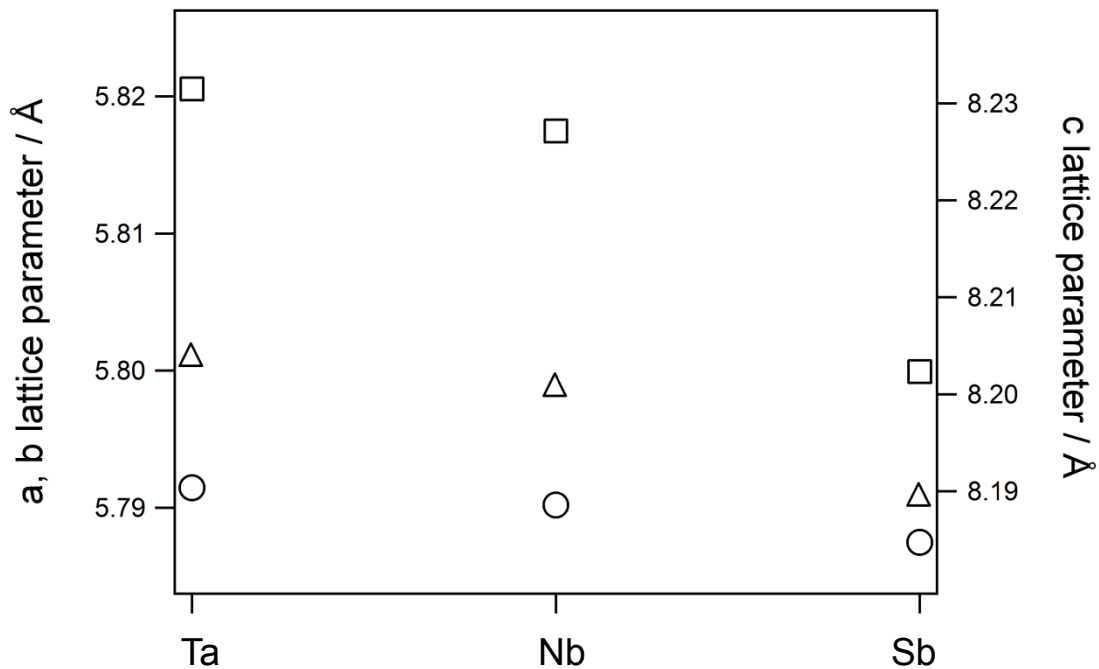23. A. M. Glazer, *Acta Cryst.* **1972,** *B28*, 3384-3392.

24. D. G. Karraker, *J. Chem. Phys.* **1971,** *55*, 1084-1086.

25. A. C. McLaughlin; M. A. de Vries; J. W. G. Bos, *Phys. Rev. B* **2010,** *82* (17), 094424-5.

26. R. D. Shannon, *Acta Cryst.* **1976,** *A 32*, 751.

27. J. A. Alonso; C. Cascales; P. Garcia Casado; I. Rasines, *J. Solid State Chem.* **1997,** *128*, 247-250.

28. H. Karunadasa; Q. Huang; B. G. Ueland; P. Schiffer; R. J. Cava, *Proceedings of the National Academy of Sciences, U.S.A* **2003,** *100*, 8097-8102.

29. W. T. Fu; D. J. W. IJdo, *J. Solid State Chem.* **2005,** *178*, 2363-2367.

30. W. T. Fu; D. J. W. IJdo, *Solid State Commun.* **2005,** *134*, 177-181.

31. H. Karunadasa; Q. Huang; B. G. Ueland; J. W. Lynn; P. Schiffer; K. A. Regan; R. J. Cava, *Phys. Rev. B* **2005,** *71* (14).

32. A. S. S. de Camargo; I. A. A. Terra; L. A. de O Nunes; M. S. Li, *J. Phys.: Condens. Matter* **2008,** *20*, 255240.

33. F. W. Karau; L. Seyfarth; O. Oeckler; J. Senker; K. Landskron; W. Schnick, *Chemistry-a European Journal* **2007,** *13* (24), 6841-6852.
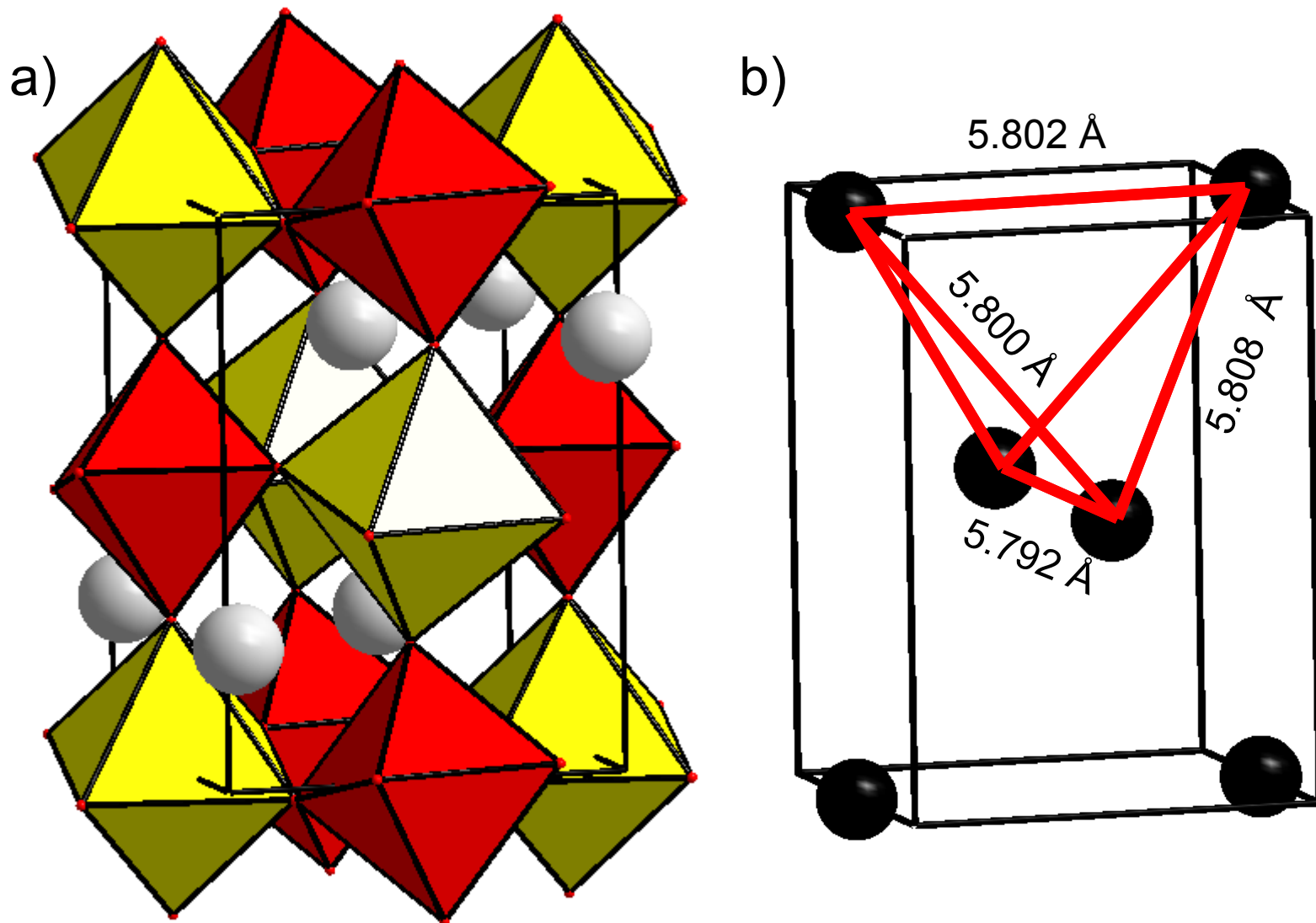
Figure 1 a) The cation-ordered perovskite structure exhibited by Sr_2YbMO_6. Grey spheres show Sr^{2+} cations whilst yellow and red octahedra represent YbO_6 and $Nb/Ta/SbO_6$ units respectively. The distortion from cubic symmetry lifts the degeneracy of the *fcc* lattice of Yb^{3+} centres, although as indicated by the distances shown in (b) the tilting of the octahedra leads to minimal distortion in the tetrahedra that compose the *fcc* lattice. The *fcc* lattice is composed of Yb^{3+} centres that are indicated by black spheres in (b).
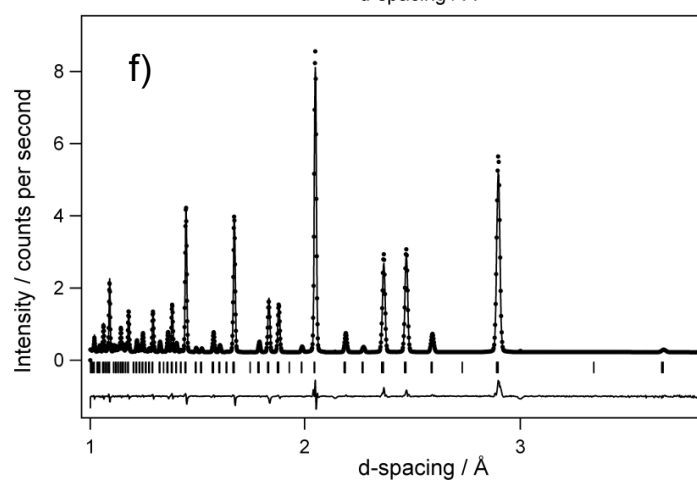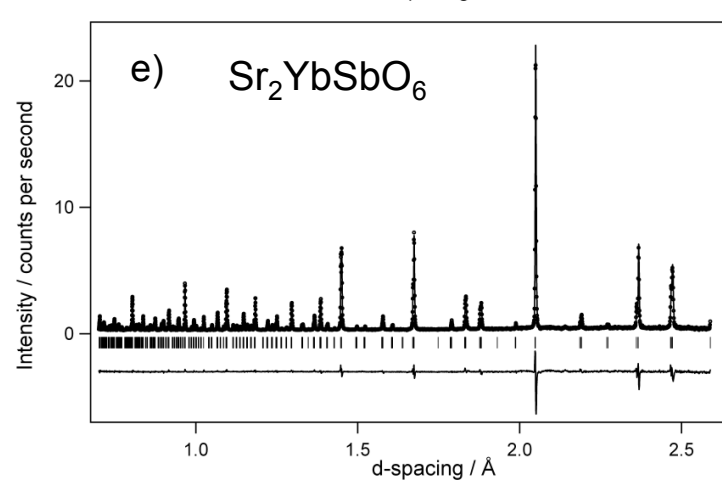
**Figure 2** Neutron time-of-flight powder diffraction patterns collected at room temperature from: (a) and (b) Sr_2YbNbO_6, (c) and (d) Sr_2YbTaO_6, (e) and (f) Sr_2YbSbO_6. Observed and calculated diffraction profiles are represented by dots and a solid line respectively. The structures were refined against two data banks simultaneously and the difference curve is illustrated.

Figure 3 The lattice parameters derived from neutron diffraction data collected at room temperature from Sr_2YbMO_6. The left hand axis indicates the values denoted by circles and squares for a and b respectively whilst c is represented by squares and the values shown on the right axis. The left and right axes are scaled such that $c/\sqrt{2}$ is comparable to the values a and b.
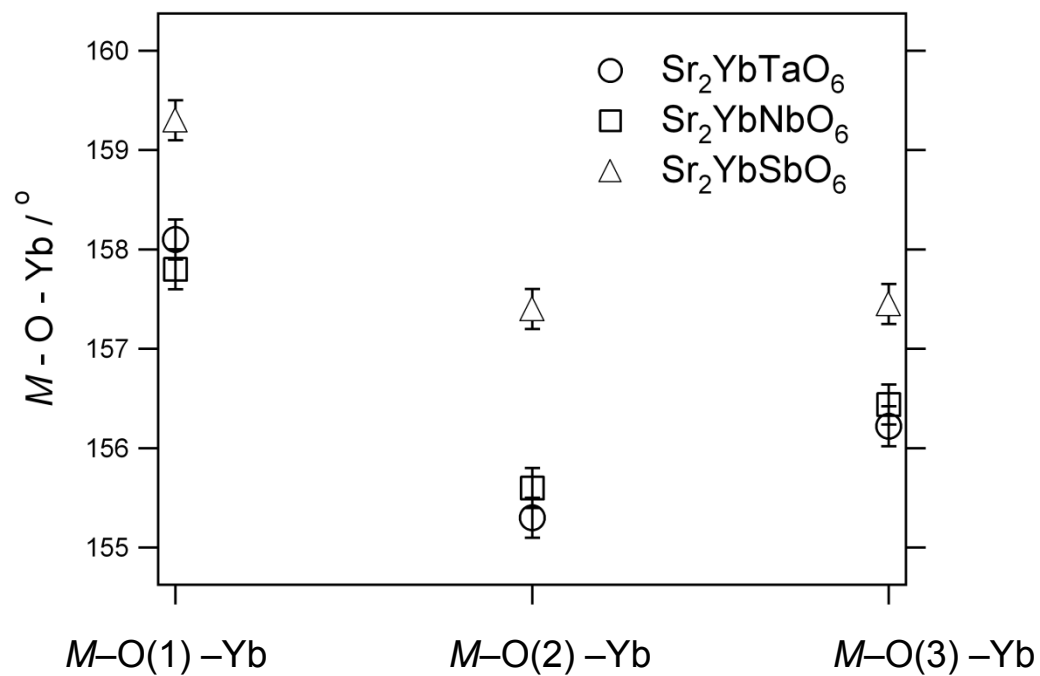
Figure 4 The M–O–Yb angles that indicate the tilting of the oxide octahedra in Sr_2YbMO_6. Circles denote values from Sr_2YbTaO_6, squares correspond to Sr_2YbNbO_6 and values from Sr_2YbSbO_6 are shown as triangles.
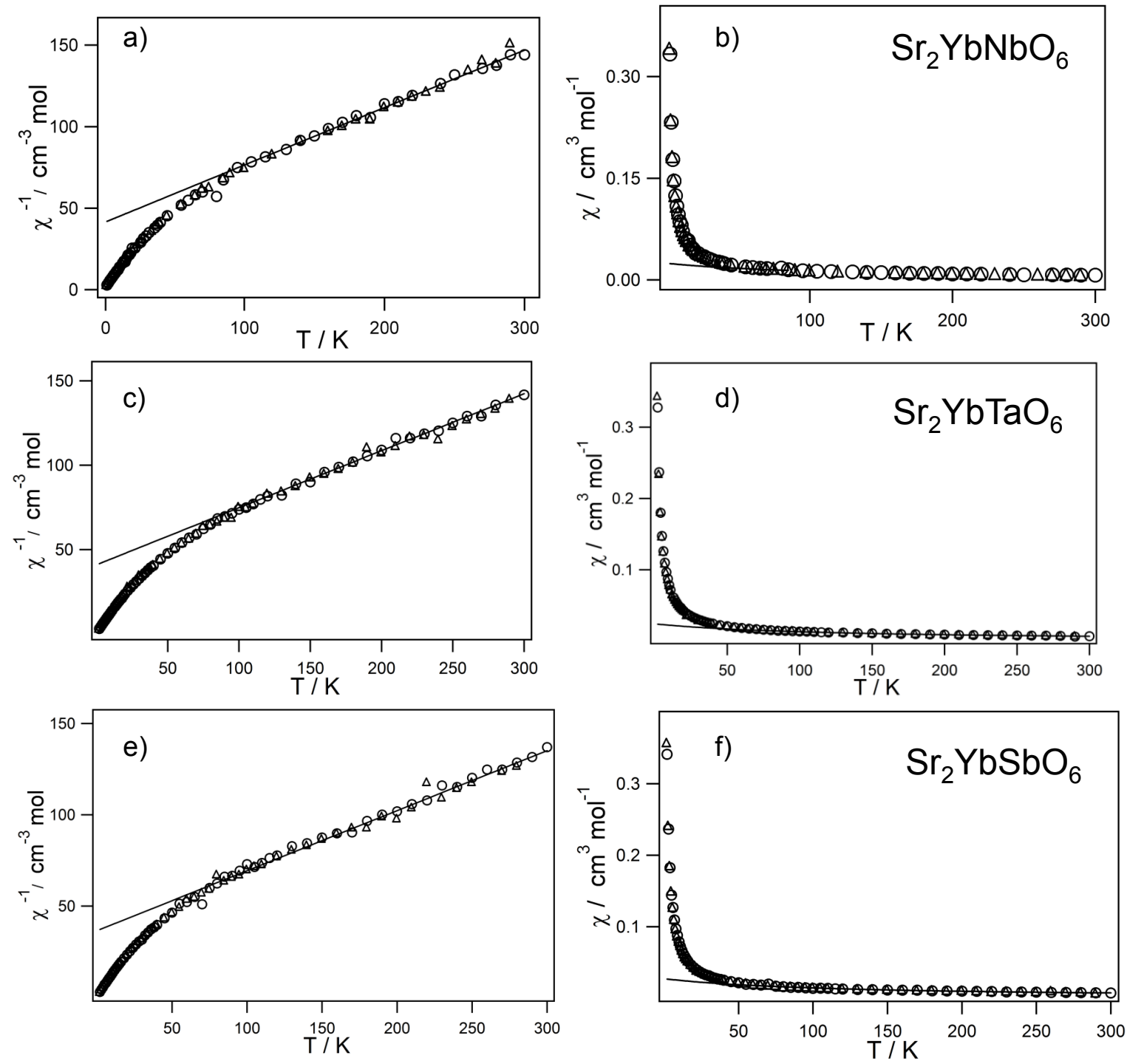
Figure 5 Magnetic susceptibility data collected from: (a) and (b) Sr2YbNbO6, (c) and (d) from Sr2YbTaO6, (e) and (f) from Sr2YbSbO6. The inverse susceptibility is shown on the left to illustrate the agreement with the Curie Weiss fit represented as a solid line. Data were collected after cooling in zero applied field (circles) and after cooling in the measuring field of 1000 G (triangles).
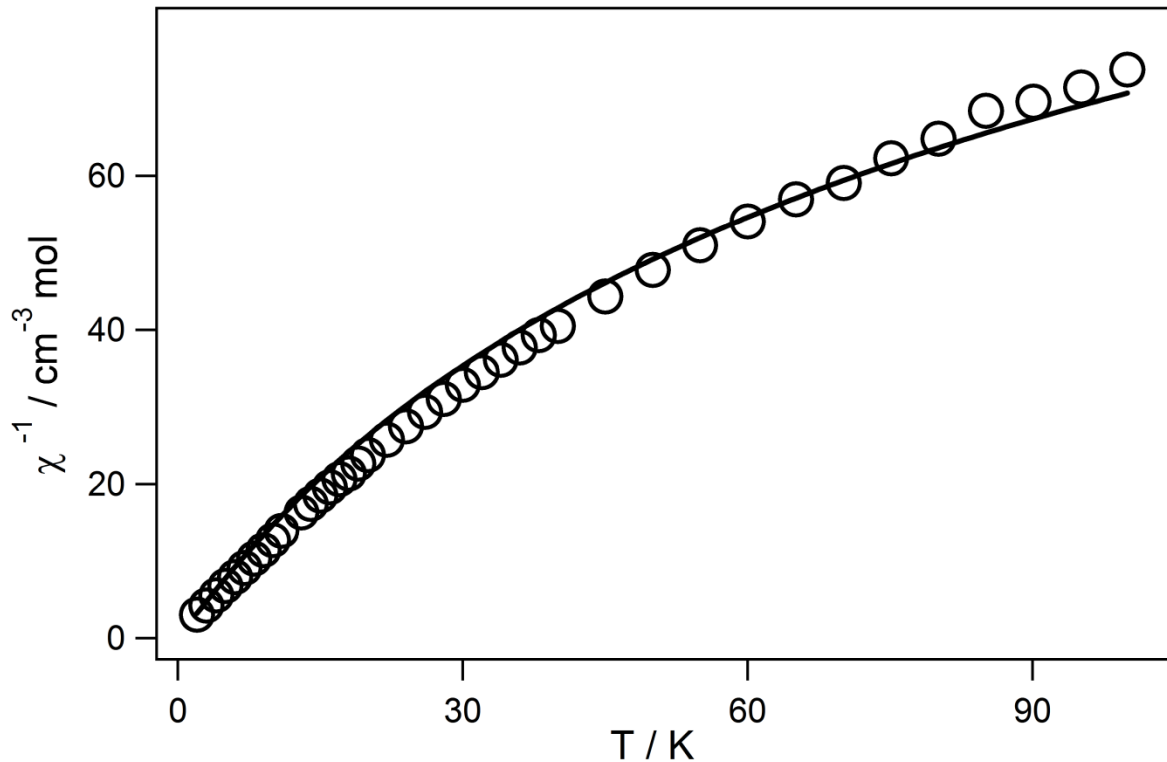
Figure 6 The inverse magnetic susceptibility of Sr_2YbTaO_6 is compared with the susceptibility calculated for Yb^{3+} in an octahedral ligand field. The black line represents the literature model based on splitting of the ground state $^2F_{7/2}$ into a Γ_6 ground state with a low lying Γ_7 level at 45 cm^{-1} higher energy. All parameters were fixed apart from the temperature independent term which refined from the value of 0.0060(2) to 0.0075(2).